Redox-Switched Bonding in Biferrocene-Containing Crown Ethers: Complexing Behavior

Teng-Yuan Dong,*[,1] Chung-Kay Chang,[1] Ching-Hung Cheng,[1] and Kuan-Jiuh Lin[2]

Department of Chemistry, National Sun Yat-Sen University, Kaohsiung, Taiwan, and the Institute of Chemistry, Academia Sinica, Nankang, Taipei, Taiwan

Received January 25, 1999

Two series of novel biferrocenes containing crown ethers have been prepared. The new compounds include 1′,1‴-bis(1,4,7,10,13-pentaoxa-16-azacyclooctadecane-16-methyl)biferrocene (**7**) and 1′,1‴-bis(1,4,7,10-tetraoxa-13-azacyclopentadecane-13-methyl)biferrocene (**8**). The complexing behavior toward alkali and alkaline earth metal cations for **7** and **8** was investigated. Solid-state structures have been determined for $NaPF_6$ and KPF_6 complexes of **8**. The reaction products of **7** and 1-(1,4,7,10,13-pentaoxa-16-azacyclooctadecane-16-methyl)ferrocene with I_2 have also been characterized by structural determinations, ^{1}H NMR, magnetic measurements, and ^{57}Fe Mössbauer technique. Complexation properties for **7** and **8** have been assessed by use of ^{1}H NMR, cyclic voltammetry measurements, and ^{57}Fe Mössbauer analyses. When the system was studied by cyclic voltammetry, new redox couples were observed in the presence of certain alkaline earth metal cations. For example, the electrochemical behavior observed for **8** with Ba^{2+} ion is fundamentally different since two new redox couples are observed for Ba^{2+} concentrations within the range $0 < [Ba^{2+}] < 2$equiv. The peak currents for the two new redox couples increase with the concentration of Ba^{2+} ion until a full equivalent is added; at this point, the original redox couples disappear and the new redox couples reach full development. This is quite unusual since compounds **7** and **8** do not have a well-formed cavity to facilitate the formation of internal metal cation complexes. Furthermore, the Mössbauer and UV/vis studies suggest no direct interaction between the iron atom and metal cation. The solid-state electron transfer in mixed-valence 1′,1‴-bis(crown ether)biferrocenium cations was also characterized by Mössbauer spectroscopy. The features in all of the Mössbauer spectra include two doublets, one with a quadrupole splitting (ΔE_Q) of ∼2.2 mms^{-1} (Fe(II) site) and the other with ΔE_Q = ∼0.4 mms^{-1} (Fe(III) site). The Mössbauer studies indicate that the electron-transfer rates in the series of mixed-valence 1′,1‴-bis(crown ether)biferrocenium cations are less than 10^7 s^{-1} in the solid state.

Introduction

The ability of macrocycles to complex a variety of cations must be considered the key property of crown ethers and cryptands.[3,4] An early goal in crown and cryptand chemistry was to see if a macrocycle's inherent cation binding could be altered by a switching mechanism. Thus far in the macrocycle field, four general switching modes have been identified: pH switch, photochemical switch, thermal switch, and oxidation−reduction switch.

Two classes of redox-switched crown ethers are known.[5] Anthraquinone-linked crown ethers show increased bonding of cations upon reduction;[6] ferrocene crown ethers on the other hand display a sharp drop in the complex stability upon oxidation.[7] In the latter case, when the ferrocene unit is incorporated within the molecular framework of the crown ether, ferrocene's d-electrons may or may not serve as donors for a bound cation, but when the ferrocene unit is oxidized, a repulsive positive charge is placed in proximity to the bound cation. Thus, ferrocene-containing crown ethers have potential as molecular sensors.

This paper reports the preparation of two new 1′,1‴-bis(crown ether)biferrocenes **1** and **2** and their complex-

(1) National Sun Yat-Sen University.
(2) Academia Sinica.
(3) (a) Gokel, G. W. *Crown Ethers and Cryptands*; Royal Society of Chemistry: London, 1991. (b) Kaifer, A. E.; Echegoyen, L. A. In *Cation Binding by Macrocyclic Systems*; Inoue, Y., Gokel, G. W., Eds.; Marcel Dekker: New York, 1990; p 363. (c) Weber, E.; Toner, J. L.; Goldberg, I.; Vögtle, F.; Laidler, D. A.; Stoddart, J. F.; Bartsch, R. A.; Liotta, C. L. In *Crown Ethers and Analogues*; Patai, S., Rappoport, Z., Eds.; John Wiley & Sons: New York, 1989. (d) Hall, C. D. *Ferrocenes*; Togni, A., Hayashi, T., Eds.; VCH: Weinheim, 1995; pp 280−316.
(4) (a) Lehn, J.-M. *Acc. Chem. Res.* **1978**, *11*, 49. (b) Runghino, G.; Romano, S.; Lehn, J.-M.; Wipff, G. *J. Am. Chem. Soc.* **1985**, *107*, 7873. (c) Lehn, J.-M. *Angew. Chem., Int. Ed. Engl.* **1988**, *27*, 89.
(5) (a) Beer, P. D. *Adv. Inorg. Chem.* **1992**, *39*, 79. (b) Beer, P. D.; Danks, J. P.; Hesek, D.; McAleer, J. F. *J. Chem. Soc., Chem. Commun.* **1993**, 2107. (c) Beer, P. D.; Crowe, D. B.; Ogden, M. I.; Drew, M. G. B.; Main, B. *J. Chem. Soc., Dalton Trans.* **1993**, 2107. (d) Lowe, N. D.; Garner, C. D. *J. Chem. Soc., Dalton Trans.* **1993**, 3333. (e) Hall, C. D.; Tucker, J. H. R.; Chu, S. Y. F.; Parkins, A. W.; Nyborg, S. C. *J. Chem. Soc., Chem. Commun.* **1993**, 1505.
(6) (a) Echegoyen, L.; Hafez, Y.; Lawson, R. C.; deMendoza, J.; Torres, T. *J. Org. Chem.* **1993**, *58*, 2009. (b) Miller, S. R.; Gustowski, D. A.; Chen, Z.; Gokel, G. W.; Echegoyen, L.; Kaifer, A. E. *Anal. Chem.* **1988**, *60*, 2021.
(7) Geiger, W. E. In *Organometallic Radical Process*; Trogler, W. C., Ed.; Elsevier: Amsterdam, 1990; p 142.

10.1021/om9900420 CCC: $18.00
Publication on Web 04/20/1999

Chart 1

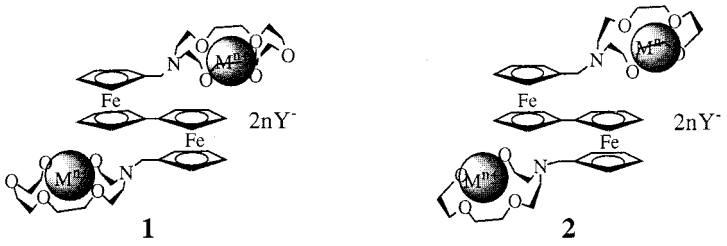

a series: $M^{n+} = Na^+$, $Y = PF_6^-$
b series: $M^{n+} = K^+$, $Y = PF_6^-$
c series: $M^{n+} = Ca^{2+}$, $Y = ClO_4^-$
d series: $M^{n+} = Ba^{2+}$, $Y = ClO_4^-$
e series: $M^{n+} = Ag^+$, $Y = PF_6^-$

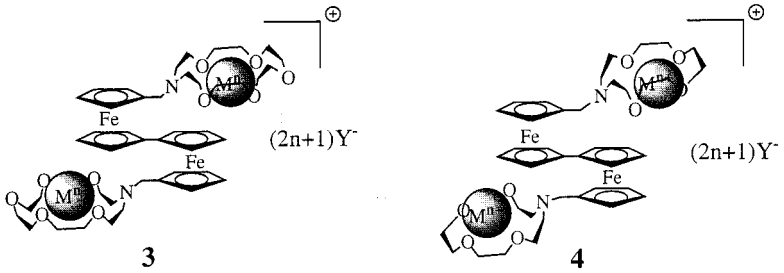

ing behavior toward alkali metals. To gain a better understanding into the factors that determine the extent of this redox-switched bonding in biferrocene-containing crown ether, we carried out X-ray crystal structural determinations, cyclic voltammetry measurements, and ^{57}Fe Mössbauer analyses. The corresponding mixed-valence 1′,1‴-bis(crown ether)biferrocenium cations **3** and **4** were also prepared and characterized by ^{57}Fe Mössbauer (see Chart 1).

Experimental Section

General Information. All manipulations involving air-sensitive materials were carried out by using standard Schlenk techniques under an atmosphere of N_2. Chromatography was performed on neutral alumina (Merck, activity II). Solvents were dried as follows: benzene, ether, and tetrahydrofuran were distilled from Na/benzophenone; dichloromethane was distilled from CaH_2; *N*,*N*,*N*′,*N*′-tetramethylethylenediamine was distilled from KOH. Samples of ferrocenium hexafluorophosphate,[8] ferrocenium perchlorate,[8] 1,1′-dibromoferrocene,[9] 1′,1‴-dibromobiferrocene,[10] ferrocenylcarboxylic acid, and biferrocenyl-1′,1‴-dicarboxylic acid[11] were prepared according to the literature procedures. As shown in Schemes 1 and 2, ferrocene-containing and biferrocene-containing crown ethers can be prepared by using corresponding bromoferrocene and 1′,1‴-dibromobiferrocene as a precursor. The physical properties of compounds are shown in Table 1.

1′,1‴-Bis(1,4,7,10,13-pentaoxa-16-azacyclooctadecane-16-carbonyl)biferrocene (5). A mixture of biferrocenyl-1′,1‴-dicarboxylic acid (0.45 g, 0.91 mmol) and excess oxalyl chloride was heated to reflux for 1 h. The volatiles were removed in a vacuum. The deep red residue was crude 1′,1‴-di(chlorocarbonyl)biferrocene, which can be used without further purification. The crude 1′,1‴-di(chlorocarbonyl)biferrocene was redissolved in dry benzene (100 mL), and this solution was transferred to a dropping funnel under nitrogen. The solution of biferrocene and a benzene solution (100 mL) of 1,4,7,10,13-pentaoxa-16-azacyclooctadecane (0.48 g, 1.8 mmol) and triethylamine (0.18 g, 1.8 mmol) in another dropping funnel were added simultaneously to a benzene solution (200 mL) under nitrogen over a period of 2 h. When addition was complete, stirring was continued for 4 h. After filtration the solvent was removed in a vacuum. The crude product was chromatographed on a column of alumina using CH_2Cl_2/CH_3OH (100:1) as the eluent. The first band was the desired compound (88% yield).

1′,1‴-Bis(1,4,7,10-tetraoxa-13-azacyclopentadecane-13-carbonyl)biferrocene (6). Preparation was analogous to that of **5**, except using 1,4,7,10-tetraoxa-13-azacyclopentadecane instead of 1,4,7,10,13-pentaoxa-16-azacyclooctadecane. Yield: 72%.

1′,1‴-Bis(1,4,7,10,13-pentaoxa-16-azacyclooctadecane-16-methyl)biferrocene (7). Reduction was effected by stirring a mixture of **5** (0.75 g, 0.79 mmol) at ambient temperature under N_2 in 20 mL of CH_2Cl_2/THF (1:2) solution with $LiAlH_4$ (118 mg, 3.16 mmol). The reaction mixture was refluxed for 3 h, then diluted with CH_2Cl_2 (50 mL), and quenched with deionized water. The organic layer was separated and washed with water (3 × 75 mL). The organic layer was then dried over $MgSO_4$. The solvent was evaporated in a vacuum. The residue was chromatographed over alumina and eluted with CH_2Cl_2/CH_3OH (100:1). The first band was the desired compound (**7**·$2H_2O$). Yield: 0.7 g (96%) of orange powder.

1′,1‴-Bis(1,4,7,10-tetraoxa-13-azacyclopentadecane-13-methyl)biferrocene (8). Preparation was analogous to that of **7**. Yield: 92%.

1′,1‴-Bis(1,4,7,10,13-pentaoxa-16-azacyclooctadecane-16-methyl)biferrocene·2(KPF$_6$)2H$_2$O (1b). The KPF_6 complex of **7** was obtained by dissolving 0.1 g (0.015 mmol) of **7** in

(8) Hendrickson, D. N.; Sohn, Y. S.; Gray, H. B. *Inorg. Chem.* **1971**, *10*, 1559.
(9) Kovar, R. F.; Rausch, M. D.; Rosenberg, H. *Organomet. Chem. Synth.* **1971**, *1*, 173.
(10) Dong, T.-Y.; Chang, C. K.; Lee, S. H.; Lai, L. L.; Chiang, Y. N. M.; Lin, K. J. *Organometallics* **1997**, *16*, 5816.
(11) Hammond, P. J.; Bell, A. P.; Hall, C. D. *J. Chem. Soc., Perkin Trans.* **1983**, *1*, 707.

Scheme 1

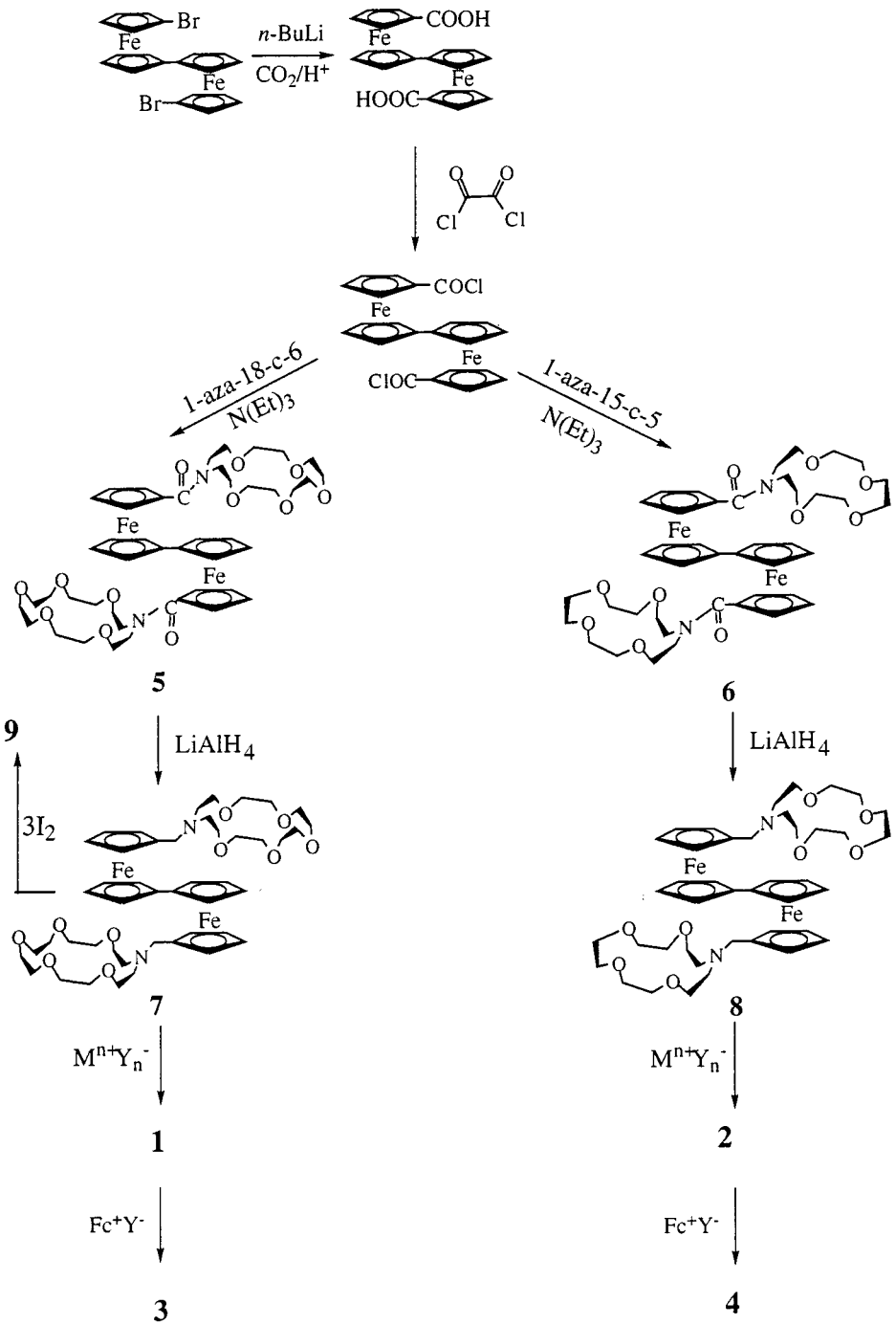

a solution containing 0.0446 g (0.243 mmol) of KPF_6 in CH_3OH (10 mL). The mixture was heated under reflux for 2 h. The solvent was removed in a vacuum. The crude product was extracted with CH_2Cl_2; then the solvent was evaporated. The product was recrystallized from C_2H_5OH to afford the product as a yellow solid (0.13 g, 98%). Anal. Calcd for $C_{46}H_{72}F_{12}Fe_2K_2N_2O_{12}P_2$: C, 41.7; H, 5.47; N, 2.11. Found: C, 41.28; H, 5.20; N, 2.20.

1′,1‴-Bis(1,4,7,10,13-pentaoxa-16-azacyclooctadecane-16-methyl)biferrocene·2Ca(ClO$_4$)$_2$·8H$_2$O (1c). The Ca$(ClO_4)_2$ complex of **7** was obtained by dissolving 0.13 g (0.141 mmol) of **7** in a solution containing 0.08 g (0.325 mmol) of Ca$(ClO_4)_2$ in CH_2Cl_2/CH_3CN (10:1, 33 mL). The mixture was stirred for 8 h. After the filtration the solvents were removed in a vacuum. The crude product was extracted with acetone. To this acetone solution was added $Na_2S_2O_3$ (0.05 g), and the mixture was then stirred for 2 h. After the filtration, the solvent was evaporated. The product was recrystallized from hexane/$CHCl_3$ (5:1) to afford the product as an orange solid (0.085 g, 43%). Anal. Calcd for $C_{46}H_{84}Ca_2Cl_4Fe_2N_2O_{34}$: C, 35.81; H, 5.49; N, 1.82. Found: C, 35.89; H, 5.43; N, 1.92.

1′,1‴-Bis(1,4,7,10,13-pentaoxa-16-azacyclooctadecane-16-methyl)biferrocene·2Ba(ClO$_4$)$_2$ (1d). A dry CH_3CN (20 mL) solution of biferrocene (0.15 g, 0.163 mmol) and Ba$(ClO_4)_2$ (0.15 g, 0.45 mmol) was refluxed 2 h under N_2. The solvent was removed in a vacuum. The crude product was extracted with CH_2Cl_2 and recrystallized from CH_2Cl_2/hexane. Yield: 0.2 g (97%) of orange powder. Anal. Calcd for $Ba_2C_{46}Cl_4Fe_2H_{68}N_2O_{26}$: C, 34.68; H, 4.30; N, 1.76. Found: C, 33.84; H, 4.51; N, 1.60.

1′,1‴-Bis(1,4,7,10,13-pentaoxa-16-azacyclooctadecane-16-methyl)biferrocene·2AgPF$_6$·8H$_2$O (1e). A dry CH_3CN solution (20 mL) of biferrocene (0.13 g, 0.141 mmol) and $AgPF_6$ (0.068 g, 0.27 mmol) was refluxed for 2 h under N_2. The solvent

Scheme 2

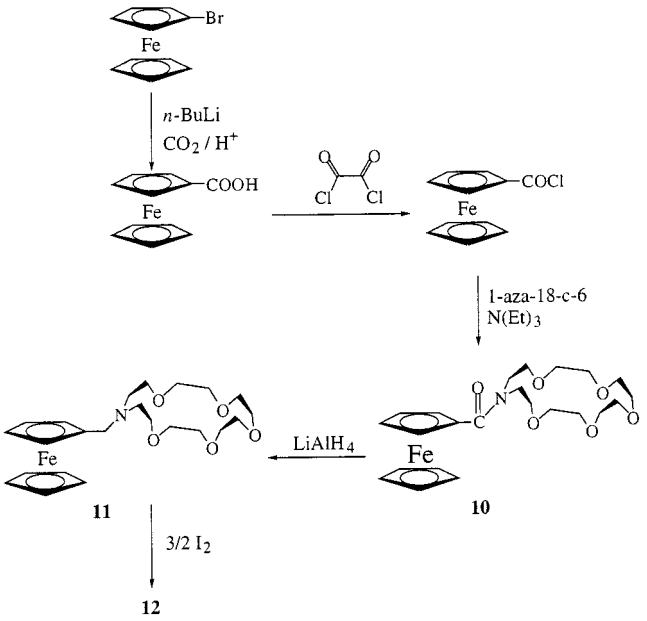

was removed in a vacuum. The crude product was extracted with $CHCl_3$ (25 mL). To this $CHCl_3$ solution was added dropwise hexane (50 mL) to afford 0.055 g of product as yellow powder (35%). Anal. Calcd for $C_{46}H_{84}Ag_2F_{12}Fe_2N_2O_{18}P_2$: C, 44.36; H, 6.15; N, 2.25. Found: C, 43.66: H, 5.50; N, 2.21.

1′,1‴-Bis(1,4,7,10-tetraoxa-13-azacyclopentadecane-13-methyl)biferrocene·2NaPF$_6$·2H$_2$O (2a). A mixture of **8** (0.07 g, 0.084 mmol) and $NaPF_6$ (0.05 g, 0.298 mmol) in CH_3OH (25 mL) was heated under reflux for 2 h. The solvent was removed in a vacuum, and the crude product was extracted with CH_2Cl_2. The CH_2Cl_2 solvent was evaporated to afford an orange solid. The product can be recrystallized from C_2H_5OH (0.097 g, 98%). Anal. Calcd for $C_{42}H_{64}F_{12}Fe_2N_2Na_2O_{10}P_2$: C, 41.88; H, 5.36: N, 2.32. Found: C, 41.48; H, 5.54; N, 2.66.

1′,1‴-Bis(1,4,7,10-tetraoxa-13-azacyclopentadecane-13-methyl)biferrocene·2KPF$_6$·C$_2$H$_5$OH (2b). Preparation was analogous to that of **2a**, using 0.08 g (0.1 mmol) of **8** and 0.05 g (0.272 mmol) of KPF_6 as starting materials. Yield: 0.11 g (97%) of orange solid. Anal. Calcd for $C_{44}H_{66}F_{12}Fe_2N_2O_9K_2P_2$: C, 42.65; H, 5.11; N, 2.37. Found: C, 43.16; H, 5.55; N, 2.63.

1′,1‴-Bis(1,4,7,10-tetraoxa-13-azacyclopentadecane-13-methyl)biferrocene·2Ca(ClO$_4$)$_2$·4H$_2$O (2c). A mixture of **8** (0.15 g, 0.18 mmol) and $Ca(ClO_4)_2$ (0.086 g, 0.36 mmol) in dry CH_3CN was stirred 3 h. The solvent was removed in a vacuum. The crude product was extracted with CH_2Cl_2. To the CH_2Cl_2 solution was added dropwise hexane to afford a yellow solid (0.125 g, 53%). Anal. Calcd for $C_{42}H_{68}Ca_2Cl_4Fe_2N_2O_{28}$: C, 36.49; H, 4.96; N, 2.03. Found: C, 35.66; H, 4.83; N, 2.09.

1′,1‴-Bis(1,4,7,10-tetraoxa-13-azacyclopentadecane-13-methyl)biferrocene·2Ba(ClO$_4$)$_2$ (2d). A mixture of **8** (0.15 g, 0.18 mmol) and $Ba(ClO_4)_2$ (0.05 g, 0.45 mmol) in dry CH_3CN (25 mL) was heated under reflux for 2 h. The solvent was removed in a vacuum. The unreacted $Ba(ClO_4)_2$ was removed with THF. The crude product was redissolved in acetone, and then hexane was added dropwise to precipitate a yellow powder (0.18 g, 67%). Anal. Calcd for $C_{42}H_{60}Ba_2Cl_4Fe_2N_2O_{24}$: C, 33.52; H, 4.02; N, 1.86. Found: C, 33.51; H, 4.07; N, 1.75.

1′,1‴-Bis(1,4,7,10-tetraoxa-13-azacyclopentadecane-13-methyl)biferrocene·2AgPF$_6$·5H$_2$O (2e). A mixture of **8** (0.15 g, 0.18 mmol) and $AgPF_6$ (0.86 g, 0.34 mmol) in acetone (25 mL) was stirred under N_2 for 2 h. The solvent was removed in vacuo. The crude product was extracted with $CHCl_3$. To the $CHCl_3$ solution was added dropwise hexane to precipitate an orange solid (0.137 g, 57%). Anal. Calcd for $C_{42}H_{70}Ag_2F_{12}Fe_2N_2O_{13}P_2$: C, 42.91; H, 6.00; N, 2.36. Found: C, 42.34; H, 4.86; N, 2.36.

1-(1,4,7,10,13-Pentaoxa-16-azacyclooctadecane-16-carbonyl)ferrocene (10). Preparation was analogous to that of **5**, using ferrocenylcarboxylic acid as starting material.

1-(1,4,7,10,13-Pentaoxa-16-azacyclooctadecane-16-methyl)ferrocene (11). Preparation was analogous to that of **7**, using **10** as starting material.

Reaction of 7 or 11 with I$_2$. A sample of **9** was prepared by adding a benzene/hexane (1:1) solution containing 3 equiv of I_2 to a benzene/hexane (1:1) solution of **7** at 0 °C. The resulting red-brown crystals were filtered and washed repeatedly with cold hexane. Recrystallization can be carried out from CH_2Cl_2/hexane. Preparation of **12** was analogous to that of **9**, using 1.5 equiv of I_2. Anal. Calcd for **9** ($C_{46}H_{68}Fe_2I_6N_2O_{10}\cdot 2H_3O$): C, 32.42; H, 4.38; N, 1.64. Found: C, 32.43; H, 4.32; N, 1.68. Anal. Calcd for **12** ($C_{23}H_{35}FeI_3NO_5\cdot H_3O$): C, 32.08; H, 4.45; N, 1.63. Found: C, 31.91; H, 4.52; N, 1.64.

Preparations of Mixed-Valence Biferrocenium Compounds (3b, 3e, 4a, 4b, and 4e). Samples of these mixed-valence compounds were prepared by stirring a mixture of 0.98 equiv of ferrocenium PF_6 and corresponding biferrocene in dry CH_2Cl_2 (10 mL) for 30 min at 0 °C. To the reaction mixture was added a solution of dry hexane (10 mL) under N_2 to precipitate a blue-purple solid. The product was recrystallized under N_2 from a CH_2Cl_2/hexane solution.

Preparations of Mixed-Valence Biferrocenium Compounds (3c, 3d, 4c, and 4d). Preparations were analogous to those of **3b**, **3e**, **4a**, **4b**, and **4e**, except using ferrocenium ClO_4 as oxidized agent and CH_2Cl_2/acetone (9:1) as solvent.

Physical Methods. ^{57}Fe Mössbauer measurements were made on a constant-velocity instrument which has been previously described.[12] The absolute temperature accuracy is estimated to be ±5 K, while the relative precision is ±0.5 K. Computer fitting of the ^{57}Fe Mössbauer data to Lorentzian lines was carried out with a modified version of a previously reported program.[13] Velocity calibrations were made using a 99.99% pure 10 μm iron foil. Typical line widths for all three pairs of iron foil lines fell in the range 0.24−0.27 mm s^{-1}. Isomer shifts are reported relative to iron foil at 300 K but are uncorrected for temperature-dependent, second-order Doppler effects. It should be noted that the isomer shifts illustrated in the figures are plotted as experimentally obtained. Tabulated data are provided.

^{1}H NMR spectra were run on a Varian VXR-300 spectrometer. Mass spectra were obtained with a VG-BLOTECH-QUATTRO 5022 system. The UV/vis spectra were recorded from 200 to 900 nm in CH_2Cl_2 by using 1.0 cm quartz cells with a Hitachi U-3501 spectrophotometer.

Electrochemical measurements were carried out with a BAS 100W system. Cyclic voltammetry was performed with a stationary Pt working electrode, which was cleaned after each run. These experiments were carried out with a 1×10^{-3} M solution of biferrocene in dry CH_3CN (1:1) containing 0.1 M of (n-C_4H_9)$_4$NPF$_6$ as supporting electrolyte. The potentials quoted in this work are relative to a Ag/AgCl electrode at 25 °C. Under these conditions, ferrocene shows a reversible one-electron oxidation wave ($E(1/2) = 0.44$ V).

The single-crystal X-ray determinations of compounds **2a**, **2b**, **9**, and **12** were carried out on an Enraf Nonius CAD4 diffractometer at 298 K. Absorption corrections were made with empirical ψ rotation. A three-dimensional Patterson synthesis was used to determine the heavy-atom positions, which phased the data sufficiently well to permit location of the remaining non-hydrogen atoms from Fourier synthesis. All non-hydrogen atoms were refined anisotropically. Hydrogen atoms were calculated at ideal distances. The X-ray crystal data are summarized in Tables 2 and 3. Tables of the final positional parameters for all atoms, the complete tables of bond

(12) Dong, T.-Y.; Schei, C. C.; Hwang, M. Y.; Lee, T. Y.; Yeh, S. K.; Wen, Y. S. *Organometallics* **1992**, *11*, 573.
(13) Lee, J. F.; Lee, M. D.; Tseng, P. K. *Chemistry* **1987**, *45*, 50.

Table 1. Physical Properties of Compounds Prepared

compd	^{1}H NMR (δ); mp; mass (m/z); IR (C−H bending); UV/vis (λ_{max}, d−d, ϵ)
5[a]	3.63−3.66 (m, 48H, 1-aza-18-c-6), 4.10 (t, 4H, Cp), 4.25 (t, 4H, Cp), 4.40 (t, 4H, Cp), 4.43 (t, 4H, Cp); 45−46 °C; 948 (M^+)
6[a]	3.64−3.66 (m, 40H, 1-aza-15-c-5), 4.12 (t, 4H, Cp), 4.26 (t, 4H, Cp), 4.41 (t, 4H, Cp), 4.49 (t, 4H, Cp); 125.5−126 °C; 844 (M^+)
7[a]	2.58 (t, 8H, −NC**H**$_2$CH$_2$O−), 3.24 (s, 4H, CpC**H**$_2$N−), 3.48 (t, 8H, −NCH$_2$C**H**$_2$O−), 3.51−3.65 (m, 32H, −OC**H**$_2$C**H**$_2$O−), 3.91 (dt, 8H, Cp), 4.12 (t, 4H, Cp), 4.23 (t, 4H, Cp); 920 (M^+)
8[a]	2.59 (t, 8H, −NC**H**$_2$CH$_2$O−), 3.24 (s, 4H, CpC**H**$_2$N−), 3.51 (t, 8H, −NCH$_2$C**H**$_2$O−), 3.62 (m, 24H, −OC**H**$_2$C**H**$_2$O−), 3.91 (dt, 8H, Cp), 4.12 (t, 4H,Cp), 4.23 (t, 4H,Cp); 84.5−85.5 °C; 832 (M^+)
1b[a]	2.45 (bs, 8H, −NC**H**$_2$CH$_2$O−), 3.09 (s, 4H, CpC**H**$_2$N−), 3.46 (bs, 8H, −NCH$_2$C**H**$_2$O−), 3.56−3.66 (m, 32H, −OC**H**$_2$C**H**$_2$O−), 4.05 (t, 4H, Cp), 4.27 (dt, 8H, Cp), 4.53 (t, 4H, Cp); 845 (cm^{-1}); 445 (nm, 5.01 × 10^2 cm^{-1} M^{-1})
1c[a]	2.49 (bs, 8H, −NC**H**$_2$CH$_2$O−), 3.59 (bs, 8H, −NCH$_2$C**H**$_2$O−), 3.70 (bs, 4H, CpC**H**$_2$N−), 3.80−3.84 (m, 32H, −OC**H**$_2$C**H**$_2$O−), 3.96 (s, 8H, Cp), 4.23 (t, 4H, Cp), 4.42 (t, 4H, Cp); 823, 844 (cm^{-1}); 390 (nm, 1.63 × 10^3 cm^{-1} M^{-1})
1d[a]	2.51 (bs, 4H, CpC**H**$_2$N−), 2.76 (bs, 8H, −NC**H**$_2$CH$_2$O−), 3.50 (bs, 8H, −NCH$_2$C**H**$_2$O−), 3.59−4.08 (m, 32H, −OC**H**$_2$C**H**$_2$O−), 4.14 (bs, 8H, Cp), 4.33 (t, 4H, Cp), 4.52 (t, 4H, Cp), 831 (cm^{-1}); 445 (nm, 1.59 × 10^3 cm^{-1} M^{-1})
1e[b]	3.62−3.75 (m, 48H, 1-aza-18-c-6), 3.87 (bs, 4H, CpC**H**$_2$N−), 4.23 (t, 4H, Cp), 4.36 (t, 4H, Cp), 4.44 (t, 4H, Cp), 4.70 (t, 4H, Cp); 844 (cm^{-1}); 445 (nm, 1.16 × 10^3 cm^{-1} M^{-1})
2a[a]	2.58 (bs, 8H, −NC**H**$_2$CH$_2$O−), 3.27 (bs, 4H, CpC**H**$_2$N−), 3.51 (bs, 8H, −NCH$_2$C**H**$_2$O−), 3.62−3.80 (m, 32H, −OC**H**$_2$C**H**$_2$O−), 3.86 (t, 4H, Cp), 4.07 (t, 4H, Cp), 4.32 (t, 4H, Cp), 4.54 (t, 4H, Cp); 837, 856 (cm^{-1}); 445 (nm, 1.37 × 10^3 cm^{-1} M^{-1})
2b[a]	2.65 (bs, 8H, −NC**H**$_2$CH$_2$O−), 3.00 (s, 4H, CpC**H**$_2$N−), 3.53 (bs, 8H, −NCH$_2$C**H**$_2$O−), 3.54−3.76 (m, 32H, −OC**H**$_2$C**H**$_2$O−), 3.93 (t, 4H, Cp), 4.02 (t, 4H, Cp), 4.27 (t, 4H, Cp), 4.41 (t, 4H, Cp); 844 (cm^{-1}); 445 (nm, 2.97 × 10^3 cm^{-1} M^{-1})
2c[a]	2.69 (bs, 4H, CpC**H**$_2$N−), 3.85−3.98 (bm, 48H, 1-aza-15-c-5, Cp), 4.27 (bs, 4H, cp), 4.53 (bs, 4H, Cp); 831, 868 (cm^{-1}); 445 (nm, 1.28 × 10^3 cm^{-1} M^{-1})
2d[b]	2.68 (bs, 4H, CpC**H**$_2$N−), 3.73−3.88 (bm, 40H, 1-aza-15-c-5), 3.98 (bs, 8H, Cp), 4.20 (bs, 4H, Cp), 4.47 (bs, 4H, Cp); 830, 857 (cm^{-1}); 445 (nm, 7.87 × 10^2 cm^{-1} M^{-1})
2e[a]	2.56 (bs, 4H, CpC**H**$_2$N−), 3.49−3.77 (bm, 40H, 1-aza-15-c-5), 3.95 (bs, 8H, Cp), 4.25 (bs, 8H, Cp), 4.43 (bs, 4H, Cp); 844 (cm^{-1}); 447 (nm, 1.04 × 10^3 cm^{-1} M^{-1})
10[a]	3.58−3.65 (m, 24H, 1-aza-18-c-6), 4.14 (s, 5H, Cp), 4.22 (t, 2H, Cp), 4.58 (t, 2H, Cp); 447 (M^+)
11[a]	2.70 (t, 4H, −NC**H**$_2$CH$_2$O−), 3.45 (s, 2H, CpC**H**$_2$N−), 3.58 (t, 4H, −NCH$_2$C**H**$_2$O−), 3.64−3.67 (m, 16H, −OC**H**$_2$C**H**$_2$O−), 4.10 (s, 5H, Cp), 4.15 (dt, 4H, Cp); 461 (M^+)
9[a]	2.76 (t, 8H, −NC**H**$_2$CH$_2$O−), 3.06 (s, 4H, CpC**H**$_2$N−), 3.58 (t, 8H, −NCH$_2$C**H**$_2$O−), 3.61−3.73 (m, 32H, −OC**H**$_2$C**H**$_2$O−), 4.28 (t, 4H, Cp), 4.29 (t, 4H, Cp), 4.46 (t, 4H, Cp), 4.71 (t, 4H, Cp)
12[a]	2.63 (t, 4H, −NC**H**$_2$CH$_2$O−), 3.16 (s, 2H, CpC**H**$_2$N−), 3.63 (t, 4H, −NCH$_2$C**H**$_2$O−), 3.61−3.73 (m, 16H, −OC**H**$_2$C**H**$_2$O−), 4.28 (s, 5H, Cp), 4.63 (t, 2H, Cp), 4.38 (t, 2H, Cp)

[a] Solvent is $CDCl_3$. [b] Sovent is acetone-*d*.

Table 2. Experimental and Crystal Data for the X-ray Structures of 2a and 2b

	2a	**2b**
formula	$C_{42}H_{60}F_{12}Fe_2N_2Na_2O_8P_2$	$C_{42}H_{60}F_{12}Fe_2K_2N_2O_8P_2$
MW	1168.54	1200.76
cryst syst	monoclinic	triclinic
space group	$P2_1/c$	$P\bar{1}$
a, Å	17.936(4)	9.115(2)
b, Å	9.464(2)	10.448(4)
c, Å	14.853(3)	15.559(4)
α, deg	90	75.04(3)
β, deg	98.36(3)	78.20(3)
γ, deg	90	65.46(3)
V, Å^3	2494.5(9)	1294.2(7)
Z	2	1
D_{calcd}, g cm^{-3}	1.556	1.541
μ, mm^{-1}	0.759	0.876
λ, Å	0.710 69	0.710 69
2θ limits, deg	45	45
max, min trans coeff	1.00, 0.89	0.995, 0.845
R1	0.058	0.0543
wR2	0.1457	0.1608

Table 3. Experimental and Crystal Data for the X-ray Structures of 9 and 12

	9	12
fomula	$C_{46}H_{74}Fe_2I_6N_2O_{12}$	$C_{23}H_{38}FeI_3NO_6$
MW	1720.21	861.11
cryst syst	triclinic	triclinic
space group	$P\bar{1}$	$P\bar{1}$
a, Å	8.416(2)	10.938(2)
b, Å	13.163(2)	11.002(3)
c, Å	13.979(2)	13.903(2)
α, deg	80.23(10)	111.680(10)
β, deg	78.03(10)	95.780(10)
γ, deg	88.40(10)	91.100(10)
V, Å^3	1501.0(5)	1543.9(6)
Z	1	2
D_{calcd}, g cm^{-3}	1.901	1.850
μ, mm^{-1}	3.615	3.517
λ, Å	0.709 30	0.709 30
2θ limits, deg	44.96	45
max, min trans coeff	0.1913, 0.4595	0.3230, 0.4697
R1	0.0492	0.0444
wR2	0.1654	0.1262

distances and angles, and thermal parameters of these compounds are given in the Supporting Information.

Structure Determination of 2a. An orange crystal (0.36 × 0.36 × 0.28 mm), which was grown by slow evaporation from a C_2H_5OH solution, was used for data collection. Cell dimensions were obtained from 20 reflections with 12.40° < 2θ < 23.08°. The θ−2θ scan technique was used to record the intensities for all reflections for which 3° < 2θ < 45°. Of the 3243 unique reflections, there were 2066 reflections with $F_o > 2.0\sigma(F_o^2)$, where $\sigma(F_o^2)$ were estimated from counting statistics.

Structure Determination of 2b. An orange crystal (0.48 × 0.38 × 0.36 mm) was obtained following the same procedure as described for **2a**. The unit cell dimensions were obtained from 20 reflections with 14.02° < 2θ < 28.50°. Data were collected to a 2θ value of 45°. Of the 3383 unique reflections, there were 2564 with $F_o > 2.0\sigma(F_o)^2$. These data were used in the final refinement of structural parameters. The structure was solved and refined as described for **2a**.

Structure Determination of 9. A red-brown crystal (0.24 × 0.20 × 0.18 mm) was obtained when a layer of hexane was allowed to slowly diffuse into a CH_2Cl_2 solution of **9**. Data were collected to a 2θ value of 44.96°. The cell dimensions were obtained from 20 reflections with 2θ in the range 19.72−26.60°. The data were also corrected for absorption with an empirical ψ rotation. Of the 3894 unique reflections, there were 3414 with $F_o^2 > 2.0\sigma(F_o^2)$. These data were used in the final refinement of the structural parameters. Structure refinement was carried out in the same manner as described for **2a**.

Structure Determination of 12. A red-brown crystal (0.28 × 0.22 × 0.20 mm) was obtained following the same procedure as described for **9**. Data were collected to a 2θ value of 45.0°. The cell dimensions were obtained from 25 reflections with

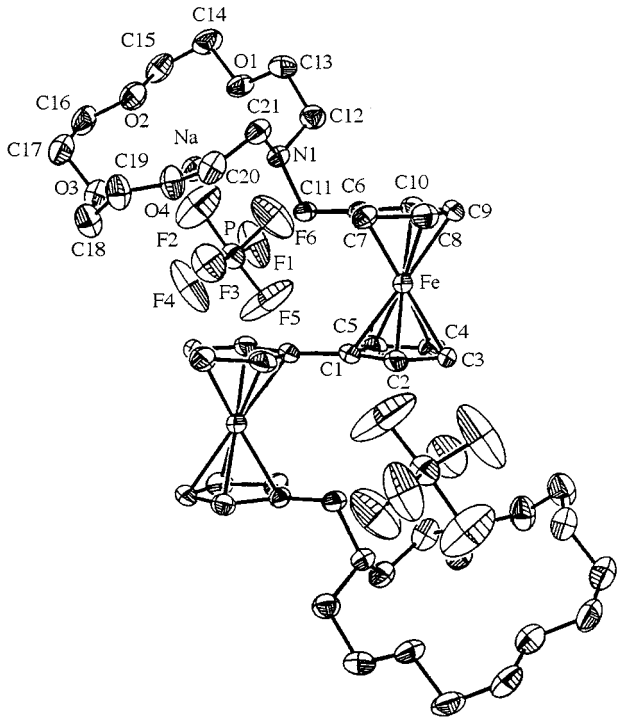

Figure 1. Molecular view of **2a** with 30% thermal ellipsoids. Hydrogen atoms have been omitted for clarity.

2θ in the range 15.9−25.10°. Of the 4042 unique reflections, there were 2898 with $F_o^2 > 2.0\sigma(F_o^2)$.

Results and Discussion

Synthesis and Characterization. The biferrocenyl derivatives described in this paper were all prepared by a similar approach. The sample of 1′,1‴-biferrocenedicarboxylic acid was converted into the diacyl chloride by treatment with oxalyl chloride. As shown in Scheme 1, the diacyl chloride was treated with 1,4,7,10,13-pentaoxa-16-azacyclooctadecane or 1,4,7,10-tetraoxa-13-azacyclopentadecane in a stoichiometric proportion for synthesis of **5** (obtained as an orange solid (mp 45−46 °C) in 88% yield) or **6** (obtained as an orange solid (mp 125.5−126 °C) in 72% yield). Reduction was carried out by stirring a mixture of **5** or **6** at ambient temperature under N_2 in 20 mL of CH_2Cl_2/THF (1:2) solution with $LiAlH_4$. Compounds **7** and **8** were obtained as orange crystals in 98% and 92% yields, respectively. Both slightly air sensitive 1′,1‴-bis(crown ether)biferrocenes were verified by mass and ^1H NMR spectroscopies.

Attempts were made to prepare a number of etherates of **7** and **8**. These included complexes with $NaPF_6$ (a series), KPF_6 (b series), $Ca(ClO_4)_2$ (c series), $Ba(ClO_4)_2$ (d series), and $AgPF_6$ (e series). In each case, 1′,1‴-bis(crown ether)biferrocene was refluxed with the appropriate metal salt in dry solvent. The complex was separated and characterized (Table 1).

Solid-State Structures of 2a and 2b. Details of the X-ray crystal data collections and unit cell parameters are given in Table 2, and their molecular structures are shown in Figures 1 and 2. Selected bond distances and angles are given in Table 4. Complete tables of positional parameters, bond distances, and bond angles are given as Supporting Information.

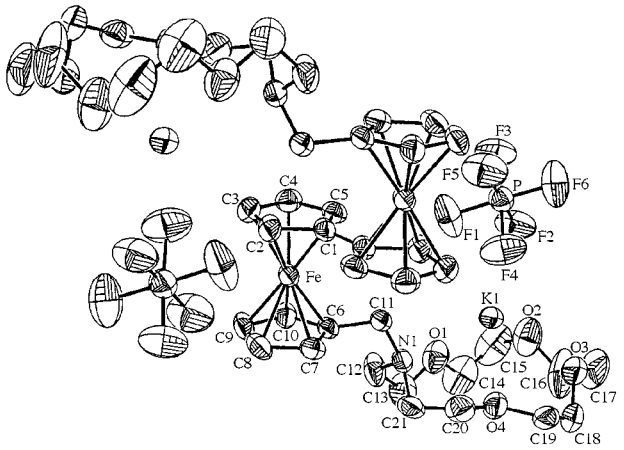

Figure 2. Molecular view of **2b** with 30% thermal ellipsoids. Hydrogen atoms have been omitted for clarity.

Table 4. Selected Bond Distances for 2a, 2b, 9, and 12

	bond angle (deg) or distance (Å)			
atoms involved	**2a**	**2b**	**9**	**12**
Fe−C	2.046(6)	2.033(5)	2.040(6)	2.025
Fe−Cp dist	1.654	1.637	1.648	1.636
C−C (Cp)	1.411(9)	1.411(9)	1.416(9)	1.40(2)
C−C (O−C−C−O)	1.48(1)	1.39(2)	1.46(2)	1.48(2)
C−C (N−C−C−O)	1.505(8)	1.48(1)	1.47(1)	1.48(1)
C−C (fc−C)	1.507(7)	1.513(7)	1.492(9)	1.48(1)
C−N (fc−C−N)	1.480(6)	1.467(6)	1.516(8)	1.528(9)
C−N (macro-ring)	1.461(7)	1.478(9)	1.53(1)	1.52(1)
M^+−N	2.520(5)	2.879(5)		
M^+−O1	2.421(5)	2.714(6)		
M^+−O2	2.438(5)	2.736(7)		
M^+−O3	2.532(5)	2.748(5)		
M^+−O4	2.351(5)	2.697(4)		
Fe−M^+	6.98	5.044		
I1−I2			2.9343(8)	2.977(1)
I1−I3			2.8882(8)	2.866(1)
I3−I1−I2			177.46(2)	

In the crystal structure of **2a** the iron atom is situated on a crystallographic center of inversion and exists in a trans conformation with the two iron ions on opposite side of the planar fulvalenide moiety. The two Cp rings in the fulvalenide moiety are crystallographically coplanar. The bond lengths and angles about the Cp rings vary little and are close to those reported for analogous ferrocenes.[14] Inspection of the average bond distance between the Fe atom and the five carbons (Fe−C) and the average Fe−Cp distance for a ferrocenyl moiety shows that these values are also close to the corresponding value observed for ferrocene (2.045 Å for Fe−C and 1.65 Å for Fe−Cp).[14] In **2a**, the two least-squares planes of the Cp rings for a given ferrocenyl moiety form a nearly parallel geometry.

When Na^+ is bound, the macro-ring adjusts to what may be considered a binding conformation in which the four Na−O distances are 2.421(5), 2.438(5), 2.532(5), and 2.351(5) Å. The average Na−O distance in **2a** is 2.436(5) Å. In known Na^+ complexes of crown ether, Na−O distances are typically in the range 2.5 ± 0.1 Å.[15] The Na−N distance in **2a** is 2.520(5) Å. An additional important observation in **2a** is that the Fe−Na distance is 6.98 Å, too long for any direct interaction.

(14) Seiler, P.; Dunitz, J. D. *Acta Crystallogr., Sect. B* **1979**, *35*, 1068.
(15) Medina, J. C.; Goodnow, T. T.; Rojas, M. T.; Atwood, J. L.; Lynn, B. C.; Kaifer, A. E.; Gokel, G. W. *J. Am. Chem. Soc.* **1992**, *114*, 10583.

In complex **2a**, the nonequivalent P−F bond lengths in the PF_6^- anion suggest an electronic interaction between Na^+ and PF_6^-. It is interesting to note that the closest Na−F2 distance of 2.516 Å is in the same range of Na−O and Na−N bond lengths. In the PF_6^- anion, the longest P−F bond distance is 1.586(5) Å (P−F2), and the P−F5 bond, which is trans to the P−F2 bond, has the shortest bond distance of 1.430(6) Å.

When K^+ is bound in the crown ether (**2b**), the molecular dimensions of the ferrocene moiety show no unusual behavior in comparison with those in **2a**. The four K−O distances are 2.714(6), 2.736(7), 2.748(5), and 2.697(4) Å. The K−N distance is 2.879(5) Å. An important observation in **2b** is that there is a special interaction between Fe^{II} and K^+. Although the ionic radii of K^+ (1.38 Å) is larger than that of Na^+ (1.02 Å), the Fe^{II}−K^+ distance in **2b** is 5.044 Å, while the Fe^{II}−Na^+ distance (6.98 Å) in **2a** is more than 1.94 Å longer. A possible explanation of this observation that does not involve a direct Fe−K interaction is that the shortened Fe−K distance is a reflection of the weaker Fe−K repulsion. There is also an interaction between K^+ and PF_6^- anion. The distances of K−F2 and K−F4 are 2.660(6) and 2.871(6) Å, respectively. In the PF_6^- anion, the distances of P−F2, P−F3, P−F4, and P−F5 are 1.568(5), 1.543(6), 1.564(5), and 1.542(5) Å, respectively.

Spectral Analysis of Cation Complexation. We apply a combination of NMR, UV, and ^{57}Fe Mössbauer techniques to study the possibility of interaction between metal cations and oxygen, nitrogen, and especially iron. Those studies could give direct observations of electronic structure when binding occurs.

^{1}H NMR Analysis of 1 and 2 Binding Na^+, K^+, Ca^{2+}, Ba^{2+}, and Ag^+. The ^{1}H chemical shift data for **1** and **2** are listed in Table 1. The spectrum may be assigned essentially in the regions δ 2.5−2.8 (−NCH_2−), 3.4−3.8 (−OCH_2−), and 4.0−4.4 (biferrocenyl protons). In ^{1}H NMR spectra of the series of **1** and **2**, the uncomplexed species are not observed, indicating that the cation exchange is faster than the NMR time scale. For the alkali and alkaline earth metal cations, the −OCH_2− chemical shift changes in the ^{1}H NMR spectra correlate qualitatively with the cation's charge density, i.e., Ca^{2+} > Ba^{2+} > Na^+ > K^+. For example, the −OCH_2− resonances observed between 3.51 and 3.65 in uncomplexed **7** move to 3.80−3.84 in **1c** complexed with Ca^{2+}. Furthermore, the −OCH_2− resonance observed at 3.62 in uncomplexed **8** move to 3.85−3.98 in **2c** complexed with Ca^{2+}. For the ferrocenyl protons (the resonances observed at 3.91, 4.12, and 4.23 in **7** shift to 3.96, 4.23, and 4.42 in **1c**), the Cp−CH_2N− protons (3.24 in **7** shift to 3.70 in **1c**), and −NCH_2− protons (2.58 in **7** shift to 2.49 in **1c**), chemical shift changes are also observed when the alkali and alkaline earth metal cations are bound. However, it is noted that the changes do not correlate qualitatively with the charge density of cation. It is possible that the coordination is dominated by the macro-ring oxygen atoms.

The ^{1}H NMR spectrum of **1e** complexed with Ag^+ is different from the others. Two chemical changes are notable. In **1e**, the larger shifts are observed for the −NCH_2−, Cp−CH_2N−, and ferrocenyl protons. The −NCH_2− resonances of **7** (free ligand), **1b** (K^+ complexed), **1c** (Ca^{2+} complexed), **1d** (Ba^{2+} complexed), and **1e** (Ag^+ complexed) are at 2.58, 2.45, 2.49, 2.76, and 3.62−3.75, respectively. The Cp−CH_2N− resonance at 3.24 in **7** (free ligand) also shifts to 3.87 in **1e**. For ferrocenyl protons, the resonances at 3.91, 4.12, and 4.23 in **7** move to 4.23, 4.36, 4.44, and 4.70 in **1e**. The macroring −OCH_2CH_2O− protons are affected little (3.51−3.65 in **7** shifted to 3.62−3.75 in **1e**). One inference can be drawn from these observations. For **1e**, the solution structure of the coordination involves the nitrogen atom to a greater extent. This interaction, however, is not a direct Ag−Fe interaction observed in ferrocenyldimethyl[2,2]cryptand (**13**) complexed with Ag^+.[15]

Chart 2

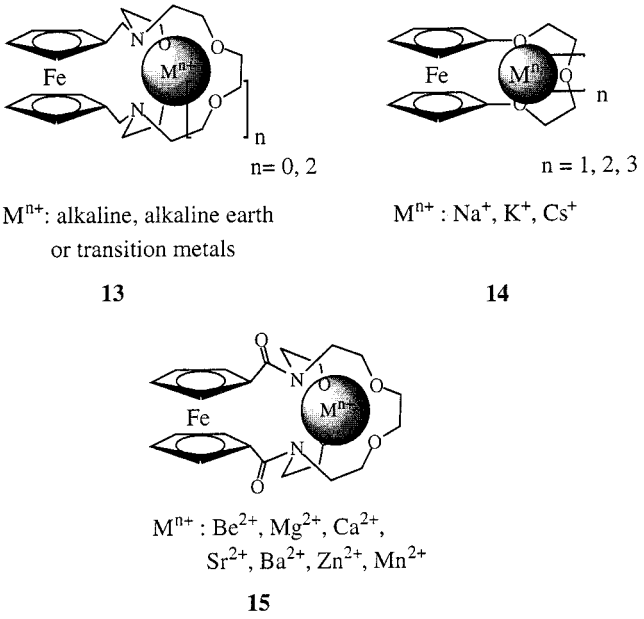

Ultraviolet Spectral Analysis of 1e. To confirm the possible existence of a direct Ag−Fe interaction, complex **1e** was examined by UV−visible spectroscopy. It is reasonable to expect that the Fe d-electrons could serve as a donor group. Furthermore, it has been known for many years that an orbital−orbital interaction between the bound Ag^+ cation and the ferrocenyl d-electrons was conformed in complexation of Ag^+ cation with ferrocenyldimethyl[2,2]cryptand. In presence of Ag^+ cation, ferrocenyldimethyl[2,2]cryptand exhibits a much larger cation-induced bathochromic red shift.[15]

For the series of **1** and **2**, the UV−visible spectra were studied in CH_3CN or CH_2Cl_2 in the range 800−200 nm (Table 1). In all but the **1c** case, λ_{max} was observed at 445 nm. In **1c** complexed with Ca^{2+}, the spectrum shows a maximum at 390 nm, exhibiting a bathochromic blue shift. These results confirm that there is no direct Fe−cation interaction. However, it is of interest to find a much larger cation-induced bathochromic blue shift in **1c**. At this moment, we cannot provide any possible explanation for this unusual observation.

^{57}Fe Mössbauer Spectral Analysis. Several groups have used Mössbauer spectroscopy to investigate possible interactions of an encapsulated cation with a ferrocenyl macrocycle. Akabori and co-workers observed[16] an increased quadrupole splitting (ΔE_Q) when

(16) (a) Akabori, S.; Shibahara, S.; Habata, Y.; Sato, M. *Bull. Chem. Soc. Jpn.* **1984**, *57*, 63. (b) Akabori, S.; Habata, Y.; Sakamoto, Y.; Sato, M.; Ebine, S. *Bull. Chem. Soc. Jpn.* **1983**, *56*, 537.

Table 5. ^{57}Fe Mössbauer Data for the Biferrocene-Containing Crown Ether (at 300 K)

compd	IS[a]	ΔE_Q[b]	Γ[c]
1b	0.423	2.312	0.255, 0.245
1c	0.429	2.317	0.308, 0.291
1d	0.440	2.232	0.592, 0.592
1e	0.426	2.321	0.334, 0.313
2a	0.441	2.358	0.365, 0.340
2b	0.423	2.304	0.398, 0.349
2c	0.423	2.273	0.265, 0.276
2d	0.423	2.298	0.274, 0.297
2e	0.418	2.294	0.284, 0.254

[a] Isomer shift referenced to iron foil in mms^{-1}. [b] Quadrupole splitting in mms^{-1}. [c] Full width at half-height taken from the least-squares-fitting program. The width for the line at more positive velocity is listed first for each doublet.

a metal ion is complexed with crown ether **14** which they have ascribed to direct interaction between the metal cation and the iron atom. In the case of **15**, no correlation of ΔE_Q values with ionic radius was evident. Hall and co-workers reported[17] that the values of isomer shift (IS) for the series of complexes **15** increase with increasing ionic radius of the group metal cations, although changes between individual complexes are small ($\pm$0.04 mms^{-1}).

The isomer shift and quadrupole splitting data for the series of **1** and **2** are given in Table 5. All of the samples gave a well-resolved quadrupole doublet in the Mössbauer spectrum, consistent with a distorted electronic structure around the ^{57}Fe nucleus. Both doublets have the same area, as deduced by a least-squares fitting. The variation in IS and ΔE_Q values through the series of **1** and **2** is not significant. Similarly, the IS and ΔE_Q values display no discernible trend. In other words, no correlation between the values of IS and ΔE_Q and the charge density of the cations is seen. We have compared the Mössbauer spectra of solid samples of **1** and **2** but detect no spectral change in our case, suggesting no direct interaction between the iron atom and metal cation.

Cyclic Voltammetric Studies of 7 in the Presence of Metal Cations. One of the most interesting attributes of **7** is the presence of a biferrocenyl redox-active moiety in proximity to the cation binding site. Binding and electron-transfer events can influence one another owing to the short distance between their respective sites. Binding events could affect the thermodynamic electron-transfer process between two iron centers in the biferrocenyl unit. Conversely, the magnitude of the electron-transfer rate in the biferrocenium unit may change the cation binding affinity. Thus, cyclic voltammetry of **7** in the presence of variable concentrations of the metal ion of choice affords a simple and effective way for estimating the communication between the redox and binding sites.

The CV studies of a 1.0 mM solution of **7** in CH_3CN/0.1 M $TBA^+PF_6^-$ show two successive one-electron oxidations (0.32 and 0.66 V vs Ag^+/Ag electrode) that correspond to the oxidation of the biferrocenyl moiety. Electrochemical reversibility is demonstrated by the peak-to-peak separation between the resolved reduction and oxidation wave maxima and 1:1 relationship of the cathodic and anodic peak currents. As shown in Table 6, addition of various concentrations of $NaPF_6$ to the same solution shifts the observed half-wave potentials; that is, the potentials of two redox couples shift gradually as the concentration of $NaPF_6$ increases until a saturation value is reached. Qualitatively similar voltammetric behavior is observed for **7** in the presence of K^+, Ca^{2+}, and Ba^{2+} ions. However, addition of 8 equiv concentration of $Ca(ClO_4)_2$ to the CH_3CN solution of **7** results in the appearance of a new set of redox waves at 0.81 V vs Ag/AgCl. This new redox couple is assigned to the process

$$(\mathbf{7}\cdot 2Ca^{2+})^+ - e^- \rightarrow (\mathbf{7}\cdot 2Ca^{2+})^{2+}$$

($E^{c2}(1/2)$ in Scheme 3)

An interesting finding is that a new set of redox couple for the $(\mathbf{7}\cdot 2Ca^{2+}) - e^- \rightarrow (\mathbf{7}\cdot 2Ca^{2+})^+$ process is not observed. This observation requires a high binding constant of the $(\mathbf{7}\cdot 2Ca^{2+})^+$ complex ($K^2 > K^1$). The large binding constant for the $(\mathbf{7}\cdot 2Ca^{2+})^+$ complex keeps this species in the solution while the potential is scanned across the $(\mathbf{7}\cdot 2Ca^{2+})^+ \rightarrow (\mathbf{7}\cdot 2Ca^{2+})^{2+}$ wave. As the potential becomes sufficiently positive to oxidize the complex, $(\mathbf{7}\cdot 2Ca^{2+})^+$ is present at a concentration level so that a new oxidation wave develops. In summary, the oxidation of **7** to $\mathbf{7}^+$ substantially increases the binding constant of the ligand. This is an unusual observation. In general, ferrocenes containing crown ethers display a sharp drop in the complex stability upon oxidation.[7] Gokel and co-workers reported a strong influence of alkali metal cations on the voltammetry of ferrocenyldimethyl[2,2]cryptand (**13**) in a relatively polar solvent such as acetonitrile.[15] The unique structural feature of compound **13** is its well-formed cavity, which facilitates the formation of internal metal cation complexes, resulting in a much stronger interaction between the ferrocenyl group and the macrocycle-bound cation. Thus, addition of substoichiometric concentrations of Na^+ to the CH_3CN solution of **13** results in the appearance of a new set of redox couple which is assigned to the process $(\mathbf{13}Na^+) \rightarrow (\mathbf{13}Na^+)^+$. Gokel also reported[15] that the oxidation of **13** to $\mathbf{13}^+$ substantially decreases the binding constant of the ligand. In our case, we would like to suggest that the electron-transfer process between two Fe centers could release the electrostatic repulsion effect between the macrocycle-bound cation and the electrogenerated positive charge on the oxidized form of the biferrocenyl unit.

The CV studies of a 1.0 mM solution of **8** in CH_3CN/0.1 M $TBA^+PF_6^-$ also show two successive one-electron oxidations (0.32 and 0.65 V vs Ag/AgCl). As given in Table 7, addition of various concentrations of Na^+ and K^+ to the CH_3CN solution of **8** shifts the observed half-wave potentials. Similarly, the voltammetric behavior in the presence of Ca^{2+} for **7** also occurred for **8**. Surprisely, the behavior observed for **8** with Ba^{2+} ion is fundamentally different since two new redox couples are observed for Ba^{2+} concentrations within the range $0 < [Ba^{2+}] < 2$ equiv. The peak currents for the two new redox couples increase with the concentration of Ba^{2+} ion until a full equivalent is added; at this point, the original redox couples disappear and the new redox couples reach full development. This indicates that the

(17) Hall, C. D.; Danks, I. P.; Hammond, P. J.; Sharpe, N. W.; Thomas, M. J. K. *J. Organomet. Chem.* **1990**, *388*, 301.

Table 6. Electrochemical Data for 7 in the Absence and in the Presence of Several Cations

M^+	equiv	$E^1(1/2)$	$E^2(1/2)$	$E^{c1}(1/2)$	$E^{c2}(1/2)$	$\Delta E(1/2)$	$\Delta E(1/2)$	$\Delta E(1/2)$
none	0	0.32	0.66					
Na^+	1	0.36	0.73					
	2	0.39	0.74					
	4	0.41	0.75					
	8	0.41	0.76			0.09	0.10	
K^+	1	0.37	0.72					
	2	0.40	0.73					
	4	0.40	0.73					
	8	0.40	0.73			0.08	0.07	
Ca^{2+}	1	0.41	0.73					
	2	0.41	0.74					
	4	0.41	0.73		0.81			
	8	0.41	0.72		0.81	0.09	0.06	0.15
Ba^{2+}	1	0.39	0.74					
	2	0.43	0.76					
	4	0.43	0.76					
	8	0.43	0.76			0.11	0.10	

Scheme 3

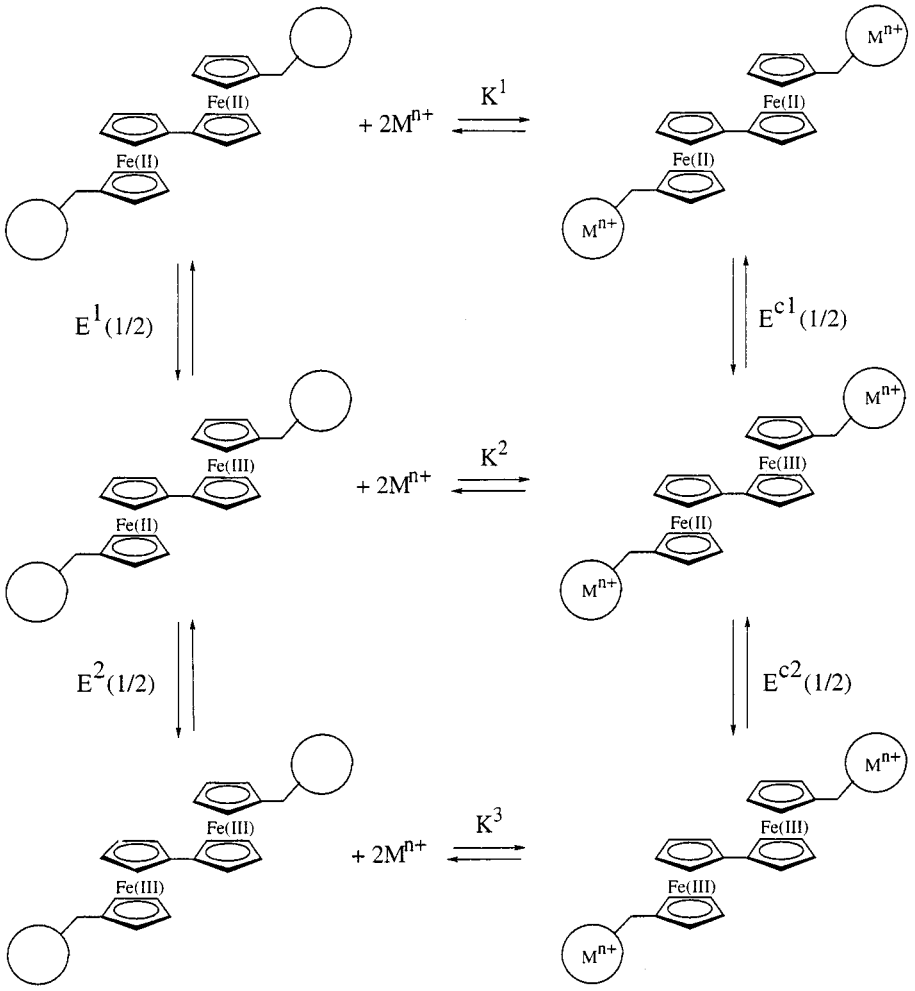

two new redox couples result from the reversible oxidation of the biferrocenyl moiety in the **8**·2Ba^{2+} complex. Compound **8** is the first reported biferrocene-based redox-active crown ether demonstrating electrochemical behavior that changed appreciably in the presence of Ca^{2+} and Ba^{2+}. This is quite unusual since compound **8** does not have a well-formed cavity to facilitate the formation of internal metal cation complexes.

Reaction Product of 7 or 11 with I_2. From the value of peak separation ($\Delta E(1/2) = 0.33$ V) between two redox couples for **7**, the disproportionation equilibrium constant K (3.92×10^5 for eq 1) can be calculated. In eq 1, the abbreviations [3,3], [2,3], and [2,2] denote the

$$[2,2] + [3,3] \overset{K}{\rightleftharpoons} 2[2,3] \qquad (1)$$

dioxidized salt, the monooxidized salt, and the neutral compound, respectively. The large value of K gives an indication of the possibility of preparing the mixed-valence biferrocenium salts.[18,19] For example, mixed-valence biferrocenium triiodide can be easily prepared by oxidizing the corresponding neutral biferrocene (K

Table 7. Electrochemical Data for 8 in the Absence and in the Presence of Several Cations

M^+	equiv	$E^1(1/2)$	$E^2(1/2)$	$E^{c1}(1/2)$	$E^{c2}(1/2)$	$\Delta E(1/2)$	$\Delta E(1/2))$
none	0	0.32	0.65				
Na^+	1	0.35	0.70				
	2	0.39	0.72				
	4	0.39	0.74				
	8	0.39	0.75			0.07	0.10
K^+	1	0.34	0.67				
	2	0.37	0.68				
	4	0.38	0.70				
	8	0.38	0.71			0.06	0.06
Ca^{2+}	1	0.43	0.76				
	2	0.42	0.75				
	4	0.42	0.75				
	8	0.42	0.75			0.10	0.10
Ba^{2+}	1	0.32	0.66	0.45	0.77		
	2			0.45	0.77		
	4			0.45	0.77		
	8			0.45	0.77	0.13	0.12

$= 1.8 \times 10^5$) with I_2.[19] Compound **9** was obtained by adding a benzene/hexane (1:1) solution containing a stoichiometric amount of I_2 to a benzene/hexane (1:1) solution of **7** at 0 °C. However, the resulting red-brown compound (**9**) is not an expected mixed-valence compound characterized by structural determination, ^{1}H NMR, magnetic measurement, and ^{57}Fe Mössbauer technique. Furthermore, the reaction product of **11** with I_2 is not a typical ferrocenium triiodide salt.

Details of the X-ray crystal data collections and unit cell parameters for **9** and **12** are given in Table 3, and their molecular structures are shown in Figures 3 and 4. Selected bond distances and angles are given in Table 4. Complete Tables of positional parameters, bond distances, and bond angles are given as Supporting Information.

As illustrated in Table 4, a direct comparison of the average Fe−C and Fe−Cp distances indicates that the ferrocenyl units in **9** and **12** are in the Fe(II) oxidation state. Inspection of the average Fe−C distance and the average Fe−Cp distance shows that these values are closer to the corresponding value observed for ferrocene[14] (2.045 Å for Fe−C and 1.65 Å for Fe−Cp) than the corresponding value observed for ferrocenium cation[20] (2.075 Å for Fe−C and 1.70 Å for Fe−Cp). In these compounds, the two least-squares planes of the Cp rings for a given ferrocenyl moiety form a nearly parallel geometry, while these two Cp rings are nearly eclipsed.

The triiodide anion is a counterion for macrocycle-bound H_3O^+ molecular cation. The I_3^- anions in **9** and **12** are essentially linear, and they also show an asymmetric structure (see Table 3). In other words, the I2 atom carries more negative charge than the other terminal I3 atom.

The Fe(II) oxidation state is also concluded from the ^{1}H NMR studies of **9** and **12**. As shown in Table 1,

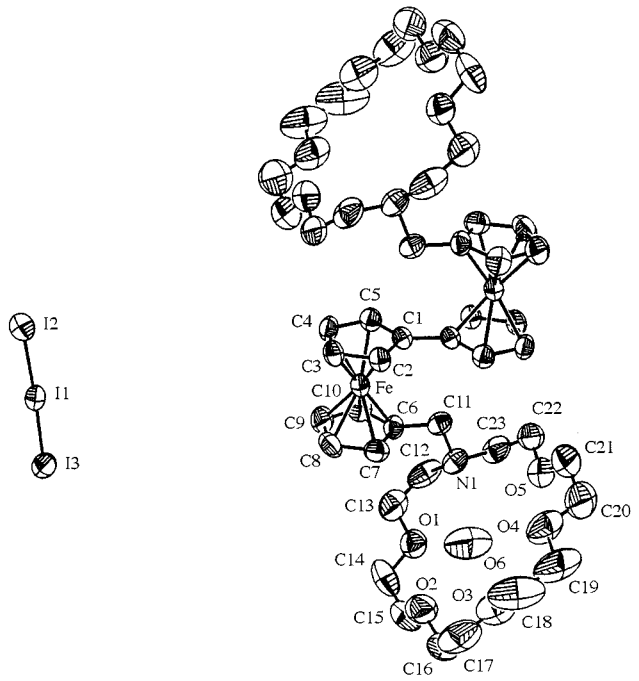

Figure 3. Molecular view of **9** with 30% thermal ellipsoids. Hydrogen atoms have been omitted for clarity.

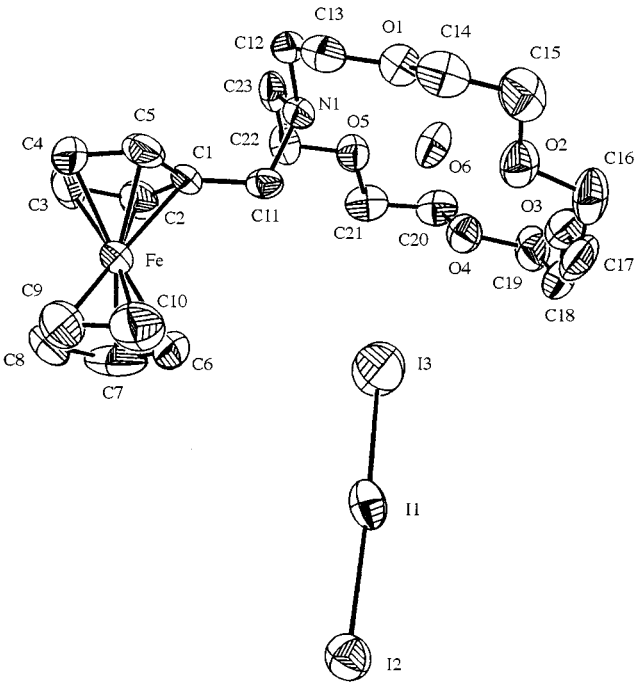

Figure 4. Molecular view of **12** with 30% thermal ellipsoids. Hydrogen atoms have been omitted for clarity.

compounds **9** and **12** exhibit typical diamagnetic NMR behavior. It has been reported that the unpaired electron in the Fe(III) ion would lead to negative spin density and positive contact shifts at the cyclopentadienyl protons. For example, three broad peaks at 16.38, 20.24, and 21.65 ppm were observed for biferrocenium triiodide.[21] Our magnetic measurements (SQUID) for **9** and **12** also indicate the presence of the Fe(II) oxidation state. In the variable-temperature magnetic susceptibility studies in the range 5−300 K, compounds

(18) (a) Morrison, W. H., Jr.; Krogsrud, S.; Hendrickson, D. N. *Inorg. Chem*. **1973**, *12*, 1998. (b) Bunel, E. E.; Campos, P.; Ruz, J.; Valle, L.; Chadwick, I.; Ana, M. S.; Gonzalez, G.; Manriquez, J. M. *Organometallics* **1988**, *7*, 474. (c) Atzkern, H.; Huber, B.; Köhler, F. H.; Müller, G.; Müller, R. *Organometallics* **1991**, *10*, 238. (d) Chukwu, R.; Hunter, A. D.; Santarisero, B. D.; Bott, S. G.; Atwood, J. L.; Chassaignac, J. *Organometallics* **1992**, *11*, 589.

(19) (a) Dong, T.-Y.; Hendrickson, D. N.; Iwai, K.; Cohn, M. J.; Rheingold, A. L.; Sano, H.; Motoyama, S. *J. Am. Chem. Soc.* **1985**, *107*, 7996. (b) Dong, T.-Y.; Huang, C. H.; Chang, C. K.; Wen, Y. S.; Lee, S. L.; Chen, J. A.; Yeh, W. Y.; Yeh, A. *J. Am. Chem. Soc.* **1993**, *115*, 6357.

(20) Mammano, N. J.; Zalkin, A.; Landers, A.; Rheingold, A. L. *Inorg. Chem*. **1977**, *16*, 297.

(21) Dong, T.-Y.; Hwang, M. Y.; Hsu, T. L.; Schei, C. C.; Yeh, S. K. *Inorg. Chem*. **1990**, *29*, 80.

Table 8. ^{57}Fe Mössbauer Least-Squares-Fitting Parameters

compd	*T*, K	IS[a]	ΔE_Q[b]	Γ[c]	peak area[d]
9	300	0.427	2.325	0.229, 0.255	
	80	0.516	2.320	0.247, 0.249	
12	300	0.430	2.341	0.377, 0.333	
	80	0.517	2.378	0.252, 0.249	
3b	270	0.468	2.221	0.286, 0.300	1.00:1.13
		0.427	0.432	0.518, 0.525	
	80	0.518	2.212	0.272, 0.265	1.00:0.53
		0.501	0.442	0.630, 0.673	
3c	270	0.459	2.168	0.300, 0.294	1.00:1.32
		0.409	0.370	0.529, 0.485	
	200	0.481	2.183	0.300, 0.311	1.00:1.06
		0.455	0.426	0.578, 0.502	
	80	0.516	2.198	0.278, 0.269	1.00:0.63
		0.515	0.413	0.702, 0.610	
3d	270	0.456	2.144	0.291, 0.316	1.00:1.60
		0.299	0.361	0.587, 0.571	
	80	0.512	2.165	0.291, 0.286	1.00:0.68
		0.490	0.442	0.577, 0.603	
3e	270	0.471	2.261	0.264, 0.257	1.00:2.45
		0.333	0.376	0.584, 0.913	
	180	0.502	2.244	0.302, 0.296	1.00:1.39
		0.406	0.426	0.609, 0.862	
	80	0.527	2.266	0.298, 0.292	1.00:0.95
		0.395	0.551	0.652, 0.869	
4a	300	0.445	2.209	0.366, 0.428	1.00:2.78
		0.334	0.309	0.673, 0.570	
	80	0.525	2.330	0.277, 0.276	1.00:0.24
		0.447	0.608	0.621, 0.643	
4b	300	0.434	2.272	0.321, 0.337	1.00:1.28
		0.324	0.282	0.689, 0.653	
	80	0.518	2.107	0.290, 0.319	1.00:1.13
		0.525	0.562	1.267, 0.852	
4c	270	0.464	2.240	0.282, 0.305	1.00:0.85
		0.398	0.452	0.607, 0.499	
	200	0.489	2.240	0.257, 0.290	1.00:0.67
		0.477	0.415	0.634, 0.553	
	80	0.512	2.231	0.288, 0.287	1.00:0.36
		0.481	0.579	0.599, 0.608	
4d	270	0.451	2.233	0.291, 0.313	1.00:1.10
		0.359	0.308	0.798, 0.521	
	180	0.497	2.221	0.280, 0.273	1.00:0.56
		0.438	0.337	0.721, 0.542	
	80	0.514	2.251	0.281, 0.271	1.00:0.34
		0.441	0.450	0.642, 0.475	
4e	270	0.471	2.207	0.288, 0.294	1.00:1.17
		0.451	0.408	0.548, 0.519	
	180	0.497	2.213	0.276, 0.280	1.00:0.84
		0.484	0.383	0.519, 0.607	
	80	0.520	2.220	0.287, 0.292	1.00:0.56
		0.509	0.448	0.509, 0.579	

[a] Isomer shift referenced to iron foil in mms^{-1}. [b] Quadrupole splitting in mms^{-1}. [c] Full width at half-height taken from the least-squares-fitting program. The width for the line at more negative velocity is listed first for each doublet. [d] The area ratio between Fe(II) doublet and Fe(III) doublet.

9 and **12** also exhibit typical diamagnetic behavior. Mössbauer spectroscopy is also a particularly useful technique for probing the oxidation state of the iron ion.[19] The ferrocenyl group gives a spectrum characterized by a large quadrupole splitting in the range 2.0−2.5 mms^{-1}, while the spectrum of the ferrocenium cation is characterized by small or vanishing quadrupole splitting. The ^{57}Fe Mössbauer spectra of **9** and **12** were obtained at 80 and 300 K. The various absorption peaks in each spectrum were fitted to Lorentzian lines, and the resulting fitting parameters are summarized in Table 8. Both compounds give a single doublet, which is expected for an Fe(II) metallocene.

As mentioned in the Experimental Section, samples of mixed-valence biferrocenium salts **3** and **4** were prepared by oxidizing the corresponding neutral biferrocene with ferrocenium cation.

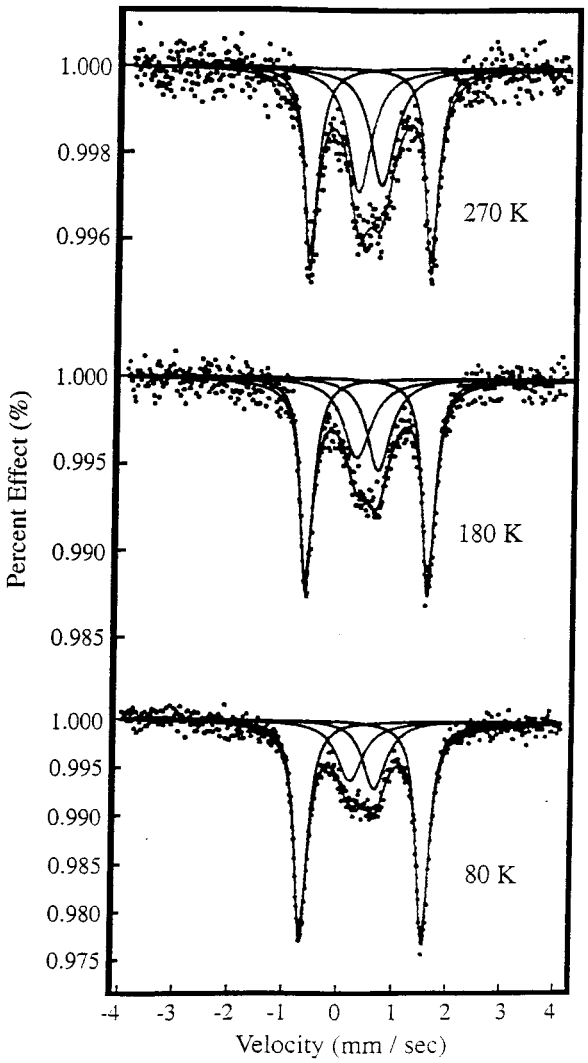

Figure 5. Variable-temperature ^{57}Fe Mössbauer spectra of mixed-valence biferrocenium **4e**.

^{57}Fe Mössbauer Characteristics of Mixed-Valence Biferrocenium 3 and 4. The rates of intramolecular electron transfer in the mixed-valence biferrocenium salts **3b**−**e** and **4a**−**e** were estimated by variable-temperature Mössbauer spectroscopy (time scale $\sim 10^7$ s^{-1}). As a typical example, the variable-temperature Mössbauer spectra of **4e** are shown in Figure 5. The various absorption peaks were fitted to Lorentzian lines. The resulting fitting parameters are collected in Table 8.

The features in all of the spectra include two doublets, one with a quadrupole splitting (ΔE_Q) of ~2.2 mms^{-1} (Fe(II) site) and the other with $\Delta E_Q = \sim 0.4$ mms^{-1} (Fe(III) site). This pattern of two doublets is expected for a mixed-valence biferrocenium cation, which is valence-trapped on the time scale of the Mössbauer experiment (electron-transfer rate $< 10^7$ s^{-1} in the solid state). However, the area ratio of Fe(III) doublet to Fe(II) doublet is quite unusual. In our case, the area ratio of Fe(III) doublet to Fe(II) doublet at 270 K is closer to 1. As the sample temperature is decreased, both doublets do not have the same area. In general, the value of the area ratio of Fe(III) doublet to Fe(II) doublet in mixed-

valence biferrocenium salts is nearly equal to 1, as deduced by a least-squares fitting.[19] We believe that the observation of temperature dependence of the area ratio is not a result of electronic effects of complexed metal ions. The variation in IS and ΔE_Q values with temperature through the series of **3** and **4** is not significant. Furthermore, the IS and ΔE_Q values display no discernible trend with the charge density of the complexed cations. Therefore, we would like to suggest that the temperature dependence of the area ratio is not a result of electronic effects of the metal ions. Here, we suggest that the temperature dependence of the area ratio is a result of slow paramagnetic relaxation in the Fe(III) site ($S = 1/2$). The electronic ground state of ferrocene is a singlet, $^2A_{1g}$ ($e_{1g}^4 a_{1g}^2$), where the one-electron molecular orbitals are predominantly d orbital in character: a_{1g} (d_{z^2}) and e_{2g} ($d_{x^2-y^2}$, d_{xy}).[22] As indicated by magnetic susceptibility[8] and EPR measurements,[23] the electronic ground state of ferrocenium is a doublet, $^2E_{2g}$ ($a_{1g}^2 e_{2g}^3$). Although there is an interaction between the nuclear spin and the electronic spin in ferrocenium, the relaxation of the latter is generally faster than the lifetime of the Mössbauer excited state so that the average value of $\langle S_z \rangle$ defined in the nuclear axis system is zero. However, if the electronic relaxation rate in ferrocenium ion is very slow at low temperature, there will again be a hyperfine interaction between the nucleus and the spin S. The electronic spin can change its quantized orientation by three types of relaxation processes: spin−spin relaxation (temperature-independent), spin−lattice relaxation (temperature-dependent), and cross-relaxation between two different spin types. The spin S may be able to couple in several ways with the nucleus. For example, the Fe(III) ($S = 1/2$) ion has a strong spin−orbital interaction, and the 4-fold degenerate $^2E_{2g}$ is also split into two Kramers' doublets. If we consider a $|\pm 1/2\rangle$ Kramers' doublet state, both the $S_z = 1/2$ and $S_z = -1/2$ orientations couple with the nuclear spin to give an observed magnetic flux density. The two Kramers' doublets of the Fe(III) ion are generally separated by only a very small energy. At high temperature two doublets are partly populated, and one can in principle expect to see two superimposed hyperfine splittings. One would expect that the lines in the ^{57}Fe Mössbauer spectra become increasingly broadened with a decrease in temperature. As shown in Figure 5 and Table 8, the Fe(III) doublet seen at 270 K becomes grossly broadened by 80 K, implying that the relaxation slows down as the temperature decreases, which is the normal situation of spin−lattice relaxation.

Acknowledgments are made to the National Science Council (NSC87-2113-M-110-010), Taiwan, ROC, and the Department of Chemistry at Sun Yat-Sen University.

Supporting Information Available: Complete tables of positional parameters, bond distances and angles, and thermal parameters for **2a**, **2b**, **9**, and **12**. Figures of voltammetric response of acetonitrile solutions containing 1.0 nM **7** or **8** and various concentrations of Ca^{2+} or Ba^{2+}. Figures of various-temperature ^{57}Fe Mössbauer spectra of **9** and **12**. This material is available free of charge via the Internet at http://pubs.acs.org.

OM9900420

(22) Duggan, D. M.; Hendrickson, D. N. *Inorg. Chem*. **1975**, *14*, 955.
(23) (a) Horsfield, A.; Wassermann, A. *J. Chem. Soc. A* **1970**, 3202. (b) Horsfield, A.; Wassermann, A. *J. Chem. Soc., Dalton Trans*. **1972**, 187. (c) Prins, R.; Kortbeek, A. *J. Organomet. Chem*. **1971**, *33*, c33.